Korean J. Chem. Eng., **25**(5), 987-997 (2008)

Effect of Ni in palladium β-zeolite on hydroisomerization of *n*-decane

Dhanapalan Karthikeyan†, Nachiappan Lingappan, and Bommasamudram Sivasankar

Department of Chemistry, Anna University, Guindy, Chennai 600025, India
(*Received 1 December 2007 • aceepted 26 Januauy 2008*)

Abstract−Bifunctional catalysts containing (0.1-0.5 wt%) Nickel and 0.1 wt% of Pd supported on H-β zeolite were synthesized by incipient wetness impregnation method and characterized by XRD, TEM, XPS, TPD and TPR techniques. The catalytic activity of Ni containing and Ni free Pd/H-β Catalysts was studied, and it was found that Ni up to a threshold value (0.3 wt% on β) produced increased the n-decane conversion and isomerization selectivity. When Ni content exceeds the threshold value, the conversion increases but isomerized products decrease. Moreover, Ni containing Pd/H-β showed increased sustainability and favored the protonated cyclopropane (PCP) intermediate mechanism in n-decane isomerization. The catalyst containing 0.3 wt% Ni 0.1 wt% Pd is adjudged as one performing better than other catalysts studied because of the isomerized mixture from it shows better octane number.

Key words: Isomerization, *n*-Decane, Zeolite-β, Ni-Pd, TPR

INTRODUCTION

The importance of *n*-alkane isomerization for improving motor fuel properties, including environmentally benign high-octane gasoline with a limited content of benzene and other aromatics, high-cetane diesel fuel with low pour and cloud points, and high viscosity lubricant base stocks with low pour points is growing [1]. Decane is one of the molecules that has been successfully used to demonstrate the mechanism of hydroisomerization-cracking reactions in the presence of bifunctional catalysts [2,3]. In all hydroisomerization processes, the metal function is due to metals, such as Pt and Pd, Re and Rh and acid function is due to supports like γ-Al_2O_3, SiO_2, clays, zeolites (β, MOR, Y, ZSM-5) [4,5] and silicoaluminophosphates (SAPO-5, SAPO-11, SAPO-41) [6]. Bimetallic catalysts have been proven to have the potential to fine-tune the heterogeneous catalysts, and have already been exploited in petroleum refining processes [7,8]. This study reports the role of Ni in light naphtha isomerization catalyzed by Ni-Pd/Hβ catalysts where the nickel was chosen as the second metal to modify the catalytic properties of the Pd catalyst, because (i) report of alloy formation between Ni and Pd, both with a common fcc lattice structure [9,10], suggesting the potentiality for interactions between the two metals, and (ii) by the addition of Ni to Pd/Hβ catalysts, the metallic-to-acid-sites ratio may be increased, thereby increasing the carbocation tolerance of the Pd catalysts. During the reaction, the noble metal catalyzes hydrogen transfer reactions (hydrogenation-dehydrogenation), while isomerization and hydrocracking occur on the Brønsted acid sites [11]. The well-accepted (classical) reaction mechanism of *n*-decane isomerization proceeds via several steps: (i) dehydrogenation on the noble metal, (ii) protonation of the *n*-alkene on the Brønsted acid site with formation of a secondary alkylcarbenium ion, (iii) rearrangement of the alkylcarbenium ion via formation of cyclic alkylcarbonium-type transition states (PCP mechanism), (iv) deprotonation, and (v) hydrogenation [12].

†To whom correspondence should be addressed.
E-mail: dkarthikeyan05@yahoo.co.in

Arifulin et al. [13] studied the effect of organic compound impurities on the hydroisomerization of decane on PdS/Al_2O_3 catalysts. Martens et al. [14] observed that H-β zeolite contains bare pores, the cages of which are slightly smaller than the supercages of faujasite and act as excellent support for Pt catalyzed in hydrocracking and hydroisomerization of long-chain alkanes to branched alkanes in the production of high-octane gasoline. The same authors [15] also reported the isomerization of decane over 0.5-1% Pt supported on ferrierite, BETA and Y zeolites. Corma et al. [16] studied hydroisomerization of *n*-decane over Pt/MSA (Mesoporous Silica Alumina), and the activity of the best Pt/MSA was compared with commercial silica alumina and USY zeolites, and the differences in the catalytic behavior were explained in terms of acidic properties and porosity. Galperin [17] investigated hydroisomerization of *n*-decane over 0.1% Pt supported on MAPO-31, SAPO-11, SAPO-34, SAPO-41, SAPO-5 and MFI. The same authors [18] observed hydroisomerization of *n*-decane in the presence of sulfur and studied the effect of metal-acid balance. Elangovan et al. [19] observed *n*-decane hydroconversion over bifunctional catalysts comprising bimetallic Pt-Pd clusters supported on an AlMCM-41 (nSi/nAl=23) mesoporous molecular sieve, where the catalytic activity of the bimetallic Pt-Pd catalysts is higher than monometallic Pt and Pd catalysts. The good balance between the two catalytic functions, namely acid sites and metal sites, also results in a higher isomer yield at a substantially lower reaction temperature. The same authors investigated [20] the hydroconversion of *n*-decane over bifunctional Pt/MCM-41//$MgAPO_{-n}$ (n-5, 11) a composite catalyst consisting of Pt/MCM-41 for the metal function and different Mg-containing aluminophosphates $MgAPO_{-n}$ for the acidic function. The highest selectivity for *n*-decane isomerization is found over a 50/50 physical mixture of 1.0 Pt/MCM-41 and MgAPO-11. Rezgui et al. [21] reported *n*-decane hydroconversion over Ni-W/SiO_2-Al_2O_3 with different Ni and W concentration (Ni ranging from 12 to 17 wt% and W ranging from 8 to 30 wt%). The products due to isomerization and cracking were functions of both metal content and acid sites up to 15 wt% of Ni. Isomerization increases subsequently due to maladjustment in the metal-acid balance. The combination of 15 wt% Ni and 10 wt%

W provided optimum balance between acid and metal functions. This catalyst is reported to give 42.3% conversion with 55% isomerization selectivity at 100 min of time on stream.

Some reports are available in the literature about the addition of Ni as the second metal to Pd, but the concentration of Ni loading kept at fairly high range (>1.0 wt%). Hence, in this present study, nickel is introduced as the second metal in low concentration range (<1.0 wt%) to modify the catalytic properties of Pd supported zeolites-β on *n*-decane hydroisomerization. Further, the present results are correlated to rationalize the variations in the product distributions in *n*-decane hydroisomerization in terms of amount of metal loading, reaction temperature and activity.

EXPERIMENTAL

1. Catalyst Preparation

The H-form of zeolite-β (SiO_2/Al_2O_3=10) was supplied by United Catalyst India Ltd., India. H-form of zeolite-β was loaded with 0.1 wt% Pd by incipient wetness impregnation (IWI) method, and the resulting materials are designated as catalysts A_1. Parts of catalysts A_1 were separately impregnated by IWI method with 0.1, 0.2, 0.3, 0.4 and 0.5 wt% Ni and the resulting samples are designated as A_2, A_3, A_4, A_5 and A_6, respectively. For comparison purpose, 0.3 wt% Ni was prepared by incipient wetness impregnation (IWI) method and the resulting materials were designated as catalyst A_7. Aqueous solutions of palladium chloride (Sisco Research Laboratory; 2×10^{-1} g Pd/ml) and nickel nitrate (Central Drug House; 5×10^{-4} g Ni/ml) were used as sources for Pd and Ni, respectively. The metal-loaded catalysts were dried at 120 °C for 24 h. Each of the earlier mentioned catalysts (1 g each) was packed in a quartz reactor and activated at 550 °C for 3 h under N_2 atmosphere. Then the temperature was lowered to 475 °C under hydrogen flow (30 ml/min/g) for 6 h in order to reduce the metal ions.

2. Characterization

2-1. X-Ray Diffraction Measurements (XRD)

The reduced A series catalysts were used for further characterization as well as for catalytic studies. The purity of zeolite-β and metal loaded zeolites were analyzed by using X'Pert X-ray diffractometer with Ni filtered Cu Kα radiation (λ=1.54 Å) in the scan range of 2θ between 5 and 80°.

2-2. Surface Area and Pore Size Distribution

BET Surface area was determined by nitrogen adsorption and desorption data acquired on a Quantachrome Autosorb Automated Gas Sorption. All the samples were pretreated in vacuum at 400 °C for 6-8 h in flowing N_2 at flow rate of 60 ml/min. Specific total surface areas were calculated by using BET and BJH equation.

2-3. Temperature Programmed Desorption (TPD)

The concentration of the acid sites was measured by temperature-programmed desorption of ammonia (TPDA) with a Micromeritics TPD/TPR 2900 analyzer. The samples (150 mg) were housed in a quartz tubular reactor and pretreated in flowing helium (≥99.9990% purity) while being heated at 10 °C/min up to the calcination temperature of the sample. After 30 min at this temperature, the samples were cooled to 210 °C and saturated for 15 min in an ammonia stream (≥99.9990% purity). The catalyst was then allowed to equilibrate in a flow at 210 °C for 1 h. Next, the ammonia was desorbed by using a linear heating rate of 15 °C/min up to 800 °C. Temperature and detector signals were simultaneously recorded. The area under the curve was integrated to determine the relative total acidity of the catalysts. Weak and strong acidities are defined as the concentration of weak and strong acid sites, respectively, obtained by integration of the area under the peaks at the lowest and the highest temperatures, respectively [22,23].

2-4. Temperature Programmed Reduction (TPR)

TPR measurements were carried out with the same apparatus as described for TPDA. After loading, the sample (150 mg) was outgassed by heating at 30 °C/min in an argon flowup to the calcination temperature of the sample and kept constant at this temperature for 30 min. Next, it was cooled to room temperature and stabilized under an argon/hydrogen flow (≥99.9990% purity, 85/15 volumetric ratio). The temperature and detector signals were then continuously recorded while heating at 20 °C/min upto 550 °C. The liquids formed during the reduction process were retained by a cooling trap placed between the sample and the detector. TPR profiles were reproducible, standard deviations for the temperature of the peak maxima being ±2%. The TPR profiles were fitted to several peaks by Gaussian deconvolution trying to keep the peak maxima constant.

2-5. X-Ray Photoelectron Spectroscopy (XPS)

The state of palladium and nickel in the catalysts A_4 and A_6 reduced at 475 °C for 6-7 h and determined by XPS. The XPS spectra were acquired with a surface analysis system (KRATOS ESCA model AXIS 165) by using the Mg Kα radiation (1253.6 eV) with 50 eV of energy. During the spectral acquisition the pressure of the analysis chamber was maintained at better than 1×10^{-7} Torr.

2-6. Transmission Electron Microscopy Analysis

TEM measurements for the reduced catalysts were carried out in JEM-2000 FX-II-JEOL 300 kV electron microscope. Specimens were enlarged by using thin photographic paper. The size of all the metal particles visible in each photograph was measured manually and averaged.

3. Catalytic Studies

The *n*-decane hydroisomerization was carried out at atmospheric pressure in a fixed bed continuous down flow quartz reactor. About 1 g of catalyst was packed and placed in a tubular furnace. The reactor system was flushed with dry nitrogen for 5 h and then the metals were reduced at 475 °C under hydrogen flow (30 ml/min/g) for 3-6 h. After reduction, the temperature was lowered to reaction temperature. The reactant *n*-decane was fed into the reactor by a syringe pump at liquid hour space velocity (LHSV)=2 h^{-1}, and pure hydrogen gas at a flow rate of 20 ml/min/g was passed with reactant and was preheated. The reaction products were passed through a condenser in ice cold condition attached to the end of the reactor and were collected in a trap kept in ice at a time interval of 1 h. The products were analyzed by AIMIL NUCON 5765 gas chromatograph equipped with a PIONA column with Flame ionization detector (FID). The products were identified by GC-MS (PERKIN ELMER QP5000).

4. Mass Balance Studies for Coke Formation

The formation of coke on the catalyst due to the effect of time-on-stream was studied by mass balance technique. The studies were carried out using 1 g of A_4 catalyst at 400 °C and LHSV=2 h^{-1}. To determine the amount of coke formed during reaction, time-on-stream studies were conducted for 15 h. In this study the catalyst was weighed before and after the experiment. The difference in weights gave the

weight gain due to coke deposition.

The spent catalyst was also calcined at 500 °C for a period of 15 h and then cooled to room temperature, and weighed. The difference between the weight of the catalyst before and after calcination was taken as the weight of coke.

RESULTS AND DISCUSSION

1. Characterization

1-1. XRD

The XRD pattern (not shown) of zeolite-β exhibits intense diffraction peaks between 2 and 50° (2θ), which is in good agreement with the standard reference [24]. The XRD patterns obtained for A series catalysts are shown in Fig. 1. The intensity of the XRD peaks decreased with the increase in Ni addition in the A series catalysts systems. Faherazzi et al. and Cullity et al. [25,26] observed the intense peaks of Pd (111,200), Ni (cubic) and NiO (hexagonal) at the 2θ values of 40, 46.5, 44.5 and 43.3° respectively, but in the present case, all these peaks were missing hence the size of the particles might be below the detection limit of XRD. Moreover intensity of the XRD peaks (A_2-A_7) at 9.7, 13.5, 19.7, 22.4, 25.8 and 26.5° (2θ) is decreased with increase in Ni addition because of pore blockage by Ni species.

1-2. NH_3-TPD

TPD profiles characterizing NH_3 adsorbed on the different catalysts are shown in Fig. 2. Peak position small vary substantially with the different metal concentration combinations. In all cases, the desorption curves were deconvoluted and fitted to two peaks, whose maximum temperatures were nearly 326 and 419 °C. These two peaks corresponded to the desorption of ammonia on weak and strong acid sites, respectively. The amount of ammonia desorbed and the desorption temperature were considered as a measure of total acidity and acid strength of catalysts, respectively [4]. It is observed from Table 1 that the amount of ammonia adsorbed at lower temperature (weak acidity) was always found to be greater than that adsorbed at higher temperature (strong acidity). Furthermore, an increase of Ni loading led to a decrease of the total acidity of the bimetallic catalysts. The decrease in acidity of the bimetallic catalysts with higher nickel loadings can be accounted for in terms of occupation of some

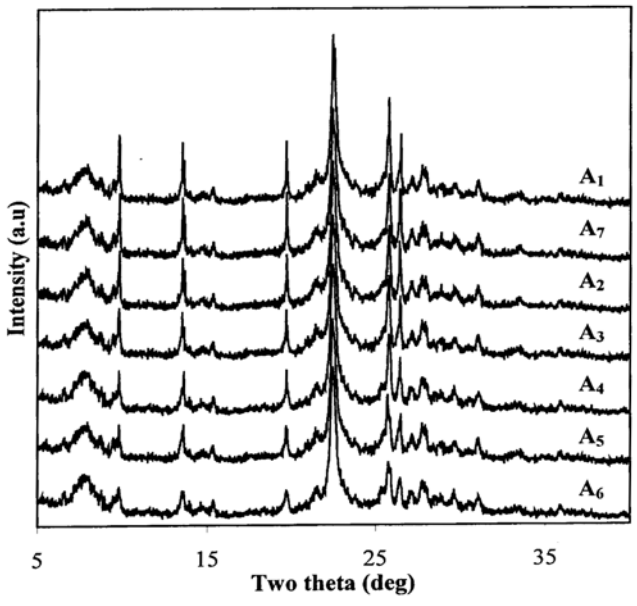

Fig. 1. XRD patterns of A series catalysts.

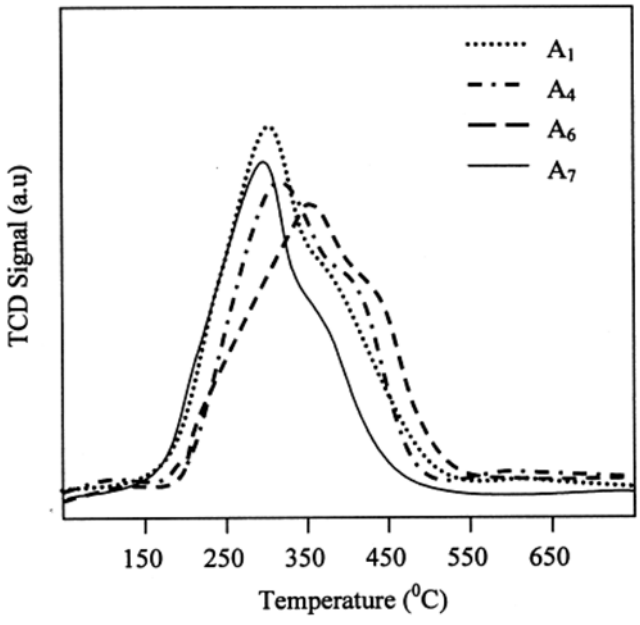

Fig. 2. NH_3-TPD curves for A_1, A_4, A_6 and A_7 catalysts.

Table 1. Physicochemical characteristics of A series catalysts

S. No	Catalyst	Pd content (wt%)	Ni content (wt%)	Surface area (m^2/g)	NH_3-TPD (mmol/g_{cat})					Particle size (nm)	Reduction temperature (°C)
					Weak acidity	T_d (°C)	Strong acidity	T_d (°C)	Total acidity		
1	A_1	0.1	-	557	0.786	283	0.128	369	0.914	-	150
2	A_2	0.1	0.1	536	0.774	294	0.103	376	0.877	-	-
3	A_3	0.1	0.2	513	0.758	298	0.087	384	0.845	-	-
4	A_4	0.1	0.3	496	0.716	307	0.068	392	0.784	4.77	130 & 410
5	A_5	0.1	0.4	466	0.704	317	0.057	408	0.761	-	-
6	A_6	0.1	0.5	448	0.684	326	0.032	419	0.716	11.73	103 & 388
7	A_7	-	0.3	497	0.724	310	0.098	354	0.822	-	420 & 580

T_d: Desorption Temperature.

acid sites by added nickel species [27-29]. This process may occur in parallel with Ni combining with Pd particles and the probable growth of Ni-Pd particles. The same results have already been reported in our previous work [29]. As shown in Table 1, a slight decrease in the values of the surface area with increasing Ni loading was also observed. This fact suggests that there would be a partial blocking of zeolite channels by the nickel species. However, it is possible to claim that a partial blocking of the zeolite micropore mouths by these species occurred because the surface area measurements were evaluated by using a small molecule like N_2 [30]. Some authors [31] found a lower acid site density and surface area when Ni was introduced in mordenite zeolite and also suggested a partial pore blockage by the Ni particles.

On the other hand, the maximum temperature corresponding to the ammonium desorption profile was marginally affected by an increase of Ni loading. This would indicate that the Ni content slightly affected the strength of acid sites (Fig. 2) [27,29].

1-3. TPR

Temperature-programmed reductions were carried out in order to determine the relative differences in the reducibility of the catalysts impregnated with different metal loadings. The TPR results of monometallic catalysts (A_1 & A_7) and bimetallic catalysts (A_4 & A_6) are presented in Table 1, and Fig. 3 illustrates the reduction profiles. Two reduction peaks at 420 and 580 °C, respectively, were detected for the sample A_7. The peak at 420 °C could be related to the reduction of NiO to Ni^0 [31]. It is very likely that some Ni^{2+} was ion-exchanged during the impregnation process [31]. It is also possible that part of the NiO particles formed during the calcinations of these catalysts react with protons of the zeolite to form $Ni(OH)^+$. The second peak at 580 °C was due to the reduction of stabilized Ni^{2+} species located into zeolite sites, where the access for H_2 molecules should be difficult [32]. Moreover, these ions located in small cavities could strongly interact with the zeolite structure in order to form less reducible species. However, in the case of the sample A_1 only one peak at 150 °C, which may be attributed to the reduction of Pd^{2+} to Pd^0 [5], was detected. On the other hand, two reduction peaks for all the bimetallic catalysts (A_4 & A_6) can be clearly noted. The first peak (130 °C) corresponds to the reduction of Pd^{2+} species, and the second peak (410 °C) to the reduction of NiO and stabilized Ni^{2+} species. For the bimetallic catalysts (A_4 and A_6), these peaks shift to lower temperatures, and the area under the highest temperature Pd peak decreases with increasing Ni content. Compared to A_7, the Ni^{2+} reduction corresponding peak was shifted to lower temperature. Similar results were obtained by Feeley and Sachtler [33] studying Pd-Ni supported in HY zeolite, and this behavior was attributed to two effects: (1) an enhanced reduction of nickel species by interaction with reduced Pd particles present in the supercages, which can dissociatively chemisorb hydrogen, and (2) a Pd-Ni ion-pair formation or by nickel ions migration from hexagonal prisms to sodalite cages containing reduced Pd atoms. Our results suggest that segregate Ni and Pd particles were mainly formed on the zeolite surface [28], although it may also be possible physical Ni-Pd bimetallic interactions.

1-4. XPS

The XPS spectra of Pd and Ni species in reduced catalysts A_4 and A_6 are shown in Fig. 4. In the case of Pd, two major peaks are observed irrespective of the support and the quantity of nickel. The peaks with binding energies of 336.4 and 342.0 eV correspond to the core level Pd $3d_{5/2}$ and Pd $3d_{3/2}$ transitions, respectively, indicating the presence of palladium in the metallic state. However, the presence of Pd in higher oxidation state cannot be avoided because of the possibility of overlap with Al 2p transition of support [34]. The XPS spectra of Ni $2p_{3/2}$ peaks have two peak maxima with binding energies 852.3 and 854.0 eV, indicating the presence of metallic nickel and NiO, respectively. A broad peak seen around 857.0 eV in A_5 indicates the presence of Ni^{2+} and the formation of $NiAl_2O_4$ from which the reduction of Ni^{2+} is very difficult (Ni metal: 852.3 eV; NiO: 853.3 eV; $NiAl_2O_4$: 857.2 eV in Phi ESCA data book). Minchev et al. [35] observed nickel remaining unreduced in their

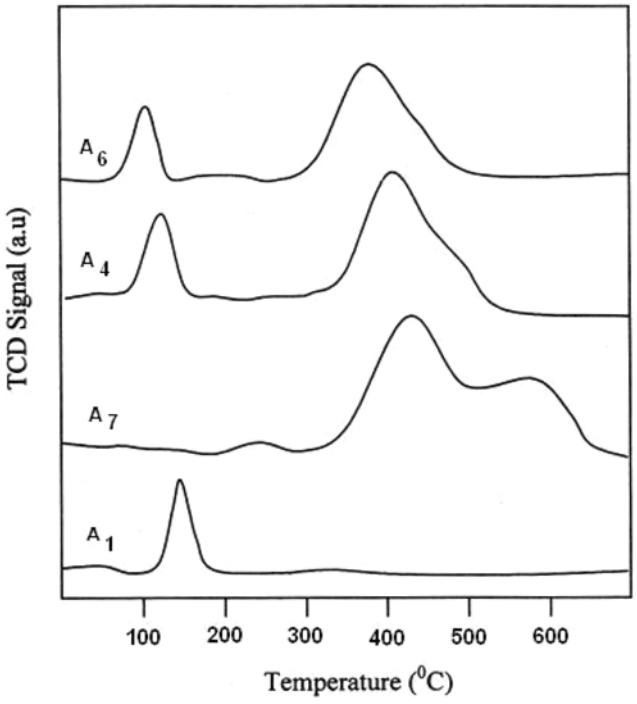

Fig. 3. TPR curves for A_1, A_4, A_6 and A_7 catalysts.

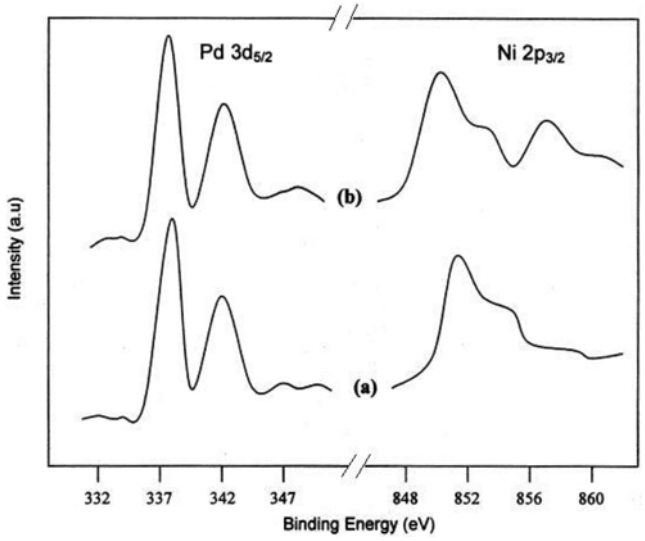

Fig. 4. XPS spectra of catalysts (a) A_4 and (b) A_6.

XPS studies of the reduction of NiY-zeolites. Further, the XPS study of Ni-mordenite by Narayanan [36] also showed that the reduction of Ni in mordenite was rather difficult, and during reduction multiple species of nickel were formed. Xiao and Meng et al. [37] analyzed the reduction and oxidation behavior of Ni containing HZSM-5 by XPS and found forms of nickel existing on the surface of the zeolite due to the interaction between Ni^{2+} and zeolite. Further, they observed the surface enrichment of aluminium and nickel. An enhanced reduction of Ni^{2+} to Ni^0 by the addition of Pd was concluded by Feely and Sachtler [33] from their TPR study on Ni/NaY-zeolite and Ni-Pd/NaY-zeolite. Thus, in the present case too, the added Pd is supposed to favor the reduction of nickel cations in the region 0-0.3 wt% Ni above which NiO is observed (for 0.5 wt%) in A series catalysts.

1-5. TEM Analysis

The TEM pictures of the catalysts, A_4 and A_6, are shown in Fig. 5. The black dots seen on the support matrix are assumed as bimetallic (Ni-Pd) particles on the surface of the supports. The average size of the particles on each support was determined and is presented in Table 1. The average particle size increased with the increase in Ni

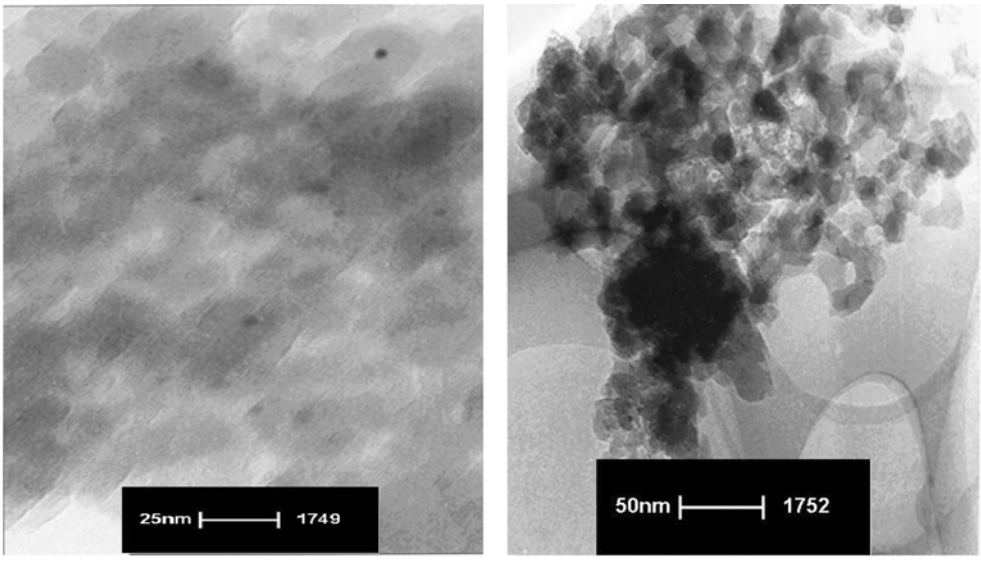

Fig. 5. TEM pictures of catalyst (a) A_4 and (b) A_6.

Table 2. Product distribution of n-decane hydroisomerization over A series of catalysts at 350 °C

Products	A_1	A_2	A_3	A_4	A_5	A_6	A_7
2-MC9	7.3	8.5	8.9	13.2	12.2	10.1	6.2
3-MC9	13.1	14.4	15.4	19.9	16.1	14.1	11.2
4-MC9	2.6	3.1	3.4	4.7	3.8	3.2	2.4
5-MC9	-	-	0.3	0.6	0.4	-	-
3-EC8	0.4	0.6	0.9	1.8	1.1	0.6	0.3
Total MBs conversion (wt%)	23.4	26.6	28.9	40.2	33.6	28.0	20.1
2,3-DMC8	3.4	4.1	4.4	5.9	4.8	3.7	3.1
2,4-DMC8	4.4	5.2	5.8	8.1	6.3	4.6	3.5
2,5-DMC8	2.9	3.8	4.0	5.2	4.3	3.1	2.7
2,6-DMC8	2.2	2.6	2.9	4.1	3.1	2.2	1.6
Total DMs conversion (wt%)	12.9	15.7	17.1	23.3	18.5	13.6	10.9
Cracked products	5.2	6.0	6.3	6.7	7.2	7.4	7.8
Conversion (wt%)	41.5	48.3	52.3	70.2	59.3	49.0	38.8
Isomerization selectivity (%)	87.5	87.6	88.0	90.5	87.9	84.9	79.9
MBs/DBs	1.8	1.7	1.7	1.7	1.8	2.1	1.8
I/C	7.0	7.1	7.3	9.5	7.2	5.6	4.0
3-MC9/2,4-DMC8	3.0	2.8	2.7	2.5	2.6	3.1	3.2

LHSV=2 h^{-1}; weight of catalyst=1 g; H_2 flow=20 ml/min/g; time on stream=1 h; MBs=Monobranched isomers; 3-EC8=3-ethyloctante; DBs=Dibranched isomers; Pressure=1 atm.

addition. Feely and Sachtler [33] from their TPR spectra characterized by a single of Ni (8.8) Pd (3.2)/NaY catalysts observed a decrease in Ni reduction temperature with the increase in Pd concentration and presumed a catalytic reduction of Ni but to mobile Palladium oxide particles colliding into each other by thermal migration and nickel oxide particles catalytically reduced by prereduced Pd particles. The average particle sizes of catalyst A_4 and A_6 were found to be 4.77 and 11.73 nm, respectively. Such particles might be larger in size compared to the pores of zeolite supports (pore size is 12MR: 5.2 Å×7.2 Å and 6.5 Å×5.6 Å) with a chance for thermal mobility during reduction, and hence may be located mainly outside the pores as reported by Romero et al. [38] in Ni/HZSM-5 catalysts. Furthermore, they reported the effect of Ni loading technique on the particle size of the Ni/HZSM-5 catalysts and observed that large particles outside the zeolite crystals are always formed, regardless of metal loading technique (ion-exchange and impregnation) by TEM studies. Hence, Ni-Pd particles might also grow in size during reduction as a result of migration of Ni towards them.

2. Catalytic Studies

Hydroisomerization of *n*-decane was carried out over the reduced bifunctional catalysts at LHSV=2 h^{-1} in the temperature range 200-450 °C in steps of 50 °C. The mono branched isomers, 2-methylnonane (2-MC9), 3-methylnonane (3-MC9), 4-methylnonane (4-MC9), 5-methylnonane (5-MC9) and 3-ethyloctane (3-E8), dibranched isomers, 2,3-dimethyloctane (2,3-DMC8), 2,4-dimethyloctane (2,4-DMC8), 2,5-dimethyloctane (2,5-DMC8) and 2,6-dimethyloctane (2,6-DMC8) were the major products due to skeletal rearrangement of carbon chain. Traces of cracked, aromatized, naphthenes and cyclized products were also observed. Products with more than ten carbon numbers were not observed. The lowest carbon numbers (C_1-C_4) were not detected under a wide range of the operating condition involved, thus excluding the existence of hydrogenolysis reaction of the feed occurring over metal sites. The product distribution of *n*-decane is presented in Table 2.

2-1. Effect of Reaction Temperature on *n*-Decane Conversion and Isomerisation Selectivity

The effect of temperature on *n*-decane conversion over all the catalytic systems is illustrated in Fig. 6. *n*-Decane conversion increased with the increase in temperature up to 400 °C, thereafter decreasing over all the catalysts. The maximum conversion of *n*-decane over all the catalytic systems was observed at 400 °C. However, the isomerization selectivity of *n*-decane over all the catalytic systems was found to increase up to 350 °C, thereafter isomerization selectivity decreased (Fig. 7). When the reaction temperature increases (from 350-450 °C), a greater amount of undesired cracked products is observed. This indicates that as temperature increases, *n*-decane is more converted to cracked products and not as isomerized products. *β*-Zeolite has three-dimensional channel structure with an aperture size (12MR: 5.2 Å×7.2 Å and 6.5 Å×5.6 Å). Thus, the structure of *β*-zeolite does not favor thermodynamically the formation of dibranched C_{10} such as 2,3-DMC8 at 200 °C and 5-MC9 and 3EC8 even at 300 °C. The formation of dibranched isomers from *n*-octane via monobranched isomers may be due to PCP intermediate as suggested by Zhang and Smirniotis [39]. The increase in isomerisation selectivity with temperature reaches a maximum at 350 °C, which is typical behavior of consecutive reactions. The rate of hydrocracking as a secondary reaction increases rapidly after 350 °C and with time on all the catalyst almost similarly. In the case of *n*-decane, catalyst A_1 showed 7.4 wt% conversion with 68.9% isomerisation selectivity at 200 °C. On increasing the temperature to 250, 300, 350 and 400 °C, the *n*-decane conversion increased to 11.1, 31.0, 41.5 and 50.8 wt% with the corresponding isomerisation selectivity 75.7, 85.2, 87.5 and 87.0%, respectively. When the reaction temperature is increased from 400 to 450 °C over the representative catalyst A_1, the conversion is found to decrease from 50.8 to 41.4 wt% with the corresponding isomerization selectivity also decreasing from 87.0 to 80.4%. The steady increase in conversion with temperature (200-400 °C) may be due to activation of the acid sites with temperature, and the isomerisation selectivity is attributed to bifunctional behavior of the acid sites with Pd particles in nanometer size. The introduction of 0.1 wt% of Ni over catalyst A_1 enhances the *n*-decane conversion and also isomerization selectivity at all temperatures. An increased *n*-decane conversion of

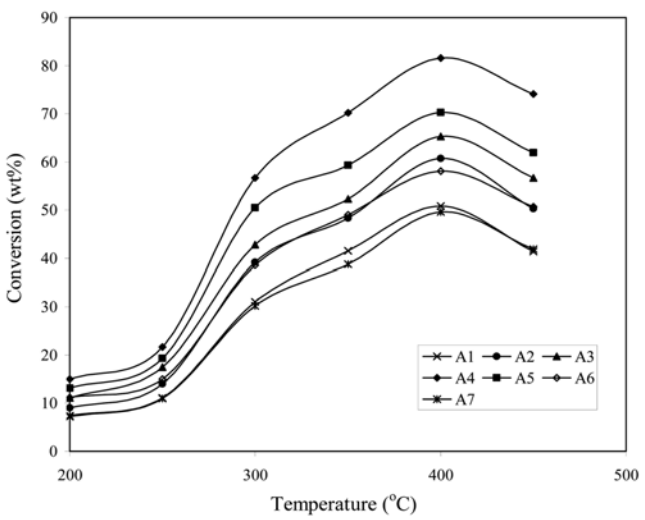

Fig. 6. Effect of temperature on *n*-decane conversion over A series catalysts.

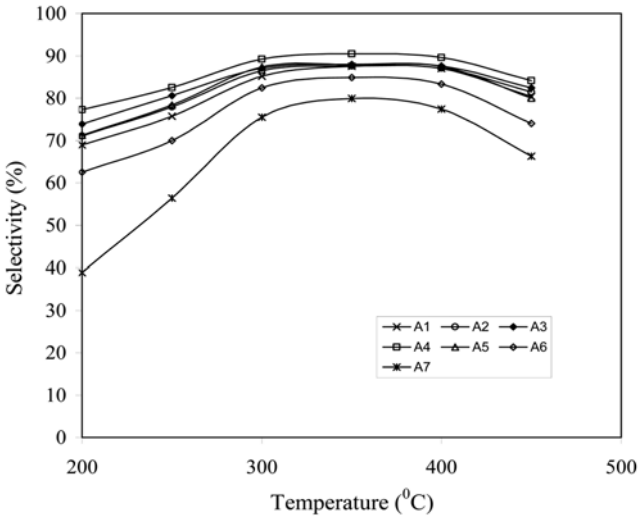

Fig. 7. Effect of temperature on the isomerization selectivity of *n*-decane over A series catalysts.

9.0, 14.0, 39.2, 48.3 and 60.7 wt% at 200, 250, 300, 350 and 400 °C, respectively, is observed over A_2, which is considerably higher than the conversion observed over catalyst A_1 at the respective temperatures. This is may be due to the activation of acid sites as explained already and also may be affected by introduction of Ni, further enhanced by the nano particle activity of the bimetallic combination Ni and Pd (both fcc forming solid solution). A small increase in the isomerization selectivity occurs when A_2 replaces A_1 (viz) 68.9, 75.7, 85.2, 87.5 and 87.0% to 71.1, 77.9, 86.5, 87.6 and 87.1% at the temperatures 200, 250, 300, 350 and 400 °C, respectively. The nano particle behavior of Ni-Pd may be the cause for small increasing isomerization selectivity also with increasing temperature. This explanation holds good for the bimetallic combination (0.3 wt% in A series). The selectivity is found to fall considerably after 350 °C for all the catalysts, when the metal combination exceeds threshold values. Thus, the fall in selectivity may be due to either larger size of the Ni-Pd combination over and above nano particles affecting the acidity of the support, or particles of oxides of Ni were not completely reduced and thus affecting the acidity on the surface of the support. In A series catalysts, 0.3 wt% Ni loaded over 0.1 wt% Pd catalyst (A_4) shows high conversion as well as isomerization selectivity at all temperatures. A similar observation was made by Jao et al. [28] in Ni-Pt/MOR and Jordao et al. [40] in Ni-Pt/HUSY over *n*-hexane isomerization. Similar trends, i.e., the increasing trend in *n*-decane conversion as well as cracking activity and small increase in isomerization selectivity with increasing reaction temperature are observed over all the remaining Pd, all Ni-Pd and Ni only loaded catalytic systems indicating the bifunctional nature of the catalysts.

2-2. Effect of Ni Addition on *n*-Decane Conversion and Isomerization Selectivity

The effect of Ni addition on *n*-decane conversion was studied by comparing the *n*-decane conversion over Ni containing and Ni free catalysts at a definite reaction temperature. The addition of 0.1 wt% Ni over 0.1 wt% Pd/Hβ enhanced the *n*-decane conversion from 7.4 to 9.0 wt% at 200 °C. The corresponding increase in conversion at 400 °C was 50.8 to 60.7 wt%. The increasing trend in conversion with Ni addition continued up to 0.3 wt% for 0.1 wt% Pd in Hβ series catalysts. Further increase of Ni content (catalyst A_5 and A_6) led to a decreasing trend in *n*-decane conversion at all the temperatures studied. A maximum conversion of 81.6 wt% was obtained over catalysts A_4 at 400 °C. Also, the Ni addition up to the above threshold values enhances the isomerization selectivity. Catalyst A_4 showed the highest isomerization selectivity of 90.5% at 350 °C, which is considerably higher than that observed over catalyst A_1 (87.5%). Further increase in Ni content over Hβ series catalysts (catalyst A_5 and A_6) led to a significant decrease in isomerization selectivity. The selectivity towards the cracking was found to be under control up to the above threshold Ni addition at all the temperatures studied. The increase in *n*-decane conversion, isomerization selectivity and cracking with increasing Ni addition is similar to the observation made by Rezgui et al. [21]. For a catalyst with higher metallic site/acid site (N_M/N_A) ratio, the diffusion distance between the two metallic sites might be shorter than a catalyst with lower (N_M/N_A) ratio. In the present case, the initial increase in conversion with suppression of cracking by increasing addition of Ni might be due to formation and growth of catalytically active Ni-Pd bimetallic particles of nanometer scale as well as better balance between the acid sites of support and bimetallic particles. The maximum activity and selectivity observed on catalyst A_4 may be due to the better metal-acid balance. The TEM studies showed that the average particle size of bimetallic particles increased with increasing Ni loading. Catalyst A_4 has an average particle size 4.77 nm by TEM analysis. Furthermore, the XPS spectrum of catalyst A_4 shows the complete reduction of Pd and Ni oxides to metallic state. The added Ni species may increase the total number of active metallic sites, i.e., the metallic sites/acid sites ratio may increase towards the optimum value for isomerization reactions. The initial increase in hydroisomerization selectivity and cracking with the increase in Ni addition is due to the availability of more metallic sites in the vicinity of acid sites enabling rapid hydrogenation of the carbenium ions and desorbing them as alkanes before they undergo for cracking reactions, i.e., the probability of cracking the olefinic intermediate during the migration from one metallic site to another site is less [41]. The decreasing conversion trend with increasing cracking observed over catalysts with higher Ni content may be due to the formation of larger bimetallic particles and presence of unreduced Ni as NiO and $NiAl_2O_4$ as evidenced by XPS. Catalyst A_6 has an average particle size of 11.73 nm by TEM analysis. Similar results were reported by Kuznets et al. [42] in *n*-octane isomerization over Pt/H-Y catalysts in which the cracking rate was decreased with increasing Pt content up to 0.6 wt% and then became independent of Pt loading. Such large bimetallic particles may block the pores of zeolites and exert restriction on the movement of bulky reaction intermediates. Also, the presence of unreduced Ni species, which are inactive in hydrogenation-dehydrogenation step, might affect the strength of the acid sites leading to lower activity. The decrease in crystallinity of the supports indicated by XRD is also responsible for the lower activity. The Ni only loaded catalyst (A_7) shows very low *n*-decane conversion with higher cracking tendency compared to catalyst A_4 all with the same amount of total metal content.

2-3. Effect of Temperature on the Selectivity of Individual *n*-Decane Isomers

The effect of temperature on the selectivity of individual *n*-decane isomers was examined over A_4 and the results are illustrated in Fig. 8. The hydroisomerization of n-decane is proposed to take place as suggested in the reaction mechanism (Scheme 1). The selectivity of the monobranched isomers 2-MC9, 3-MC9, 4-MC9, 5-MC9 and 3-EC8, is found to increase with increasing temperature up to 300 °C, thereafter decreasing over all the catalysts. The selectivity of 2-MC9 decreased more than that of 3-MC9, and the selectivity of 3-MC9 was higher than 2-MC9. The formation of 2-MC9 isomer is disfavored, 3-MC9 isomer being more easily formed. This has been observed by Steijns et al. [43]. in the hydroisomerization of *n*-dodecane and was found to be a general feature in the hydroisomerization of *n*-alkane (especially those with nine carbon atoms or more) which is best explained by the PCP mechanism for isomerisation [44]. The presence of 3-EC8 over many of the catalysts even at very low conversion cannot be explained by protonated cyclopropane mechanism through which 3-EC8 cannot be formed. The primary formation of 3-EC8 can almost probably be explained by the participation of type B isomerization reaction of protonated cyclobutane intermediates (PCB) as proposed by Martens and Jacobs [45]. The selectivity of dibranched isomers 2,3-DMC8, 2,4-DMC8, 2,5-DMC8 and 2,6-DMC8, increased with the increase in temperature.

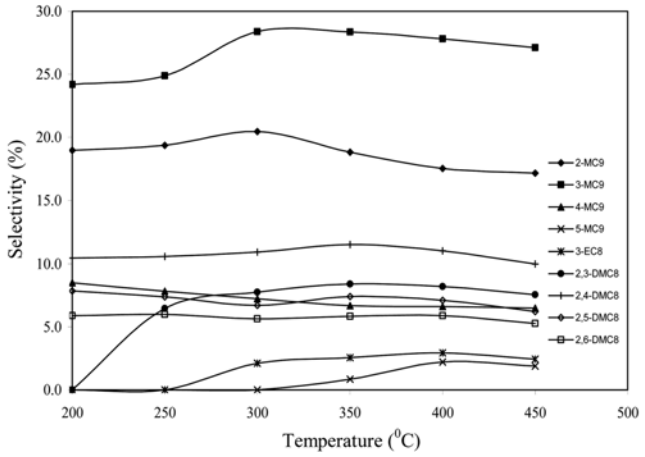

Fig. 8. Effect of temperature on the selectivity of individual *n*-decane isomers over A_4 catalyst.

Among these dibranched isomers, the selectivity of 2,4-DMC8 is higher than the other dibranched isomers (2,3-DMC8, 2,5-DMC8 and 2,6-DMC8). The presence data indicate that the predominant dibranched isomers were those with distant methyl groups (2,3-DMC8 and 2,4-DMC8). This is because, as for the first branching, the less bulky PCP intermediate during the second branching are strongly favored, explaining the low selectivities for dibranched isomer with proximate methyl groups [46]. According to Lucas et al. [47], the dibranched decane isomer due to the bulkier transition state, intermediates of isomers such as 2,2-dimethyloctane and 3,3-dimethyloctane with two branches on the same carbon of the main chain, their formation is favored in zeolites without steric hindrance for the diffusion of products. For zeolites with relatively large pores such as beta zeolite the presence of these isomers was more abundant. The increase in the formation of dibranched isomers with increase in temperature, as well as the conversion, indicates that the dibranched isomers are secondary products formed from primary monobranched isomers by protonated cyclopropane intermediate formation. Similar results have already been reported in our previous work [27,29]. With respect to tribranched isomers, they were not detected as final products over all the catalysts investigated in this work. This is because of the relatively high temperatures, which do not favor thermodynamically the formation of tribranched isomers. Moreover, the fast cracking of the latter hydrocarbons is responsible for the absence of tribranched isomers in the final products [39]. The selectivity of monobranched isomers is higher than dibranched isomers. The earlier observations indicate that the pore structure, size and kinetic diameter of the reactants, products and intermediates were responsible for the difference in the selectivity of dibranched isomers. Zeolite-β has three-dimensional linear chan-

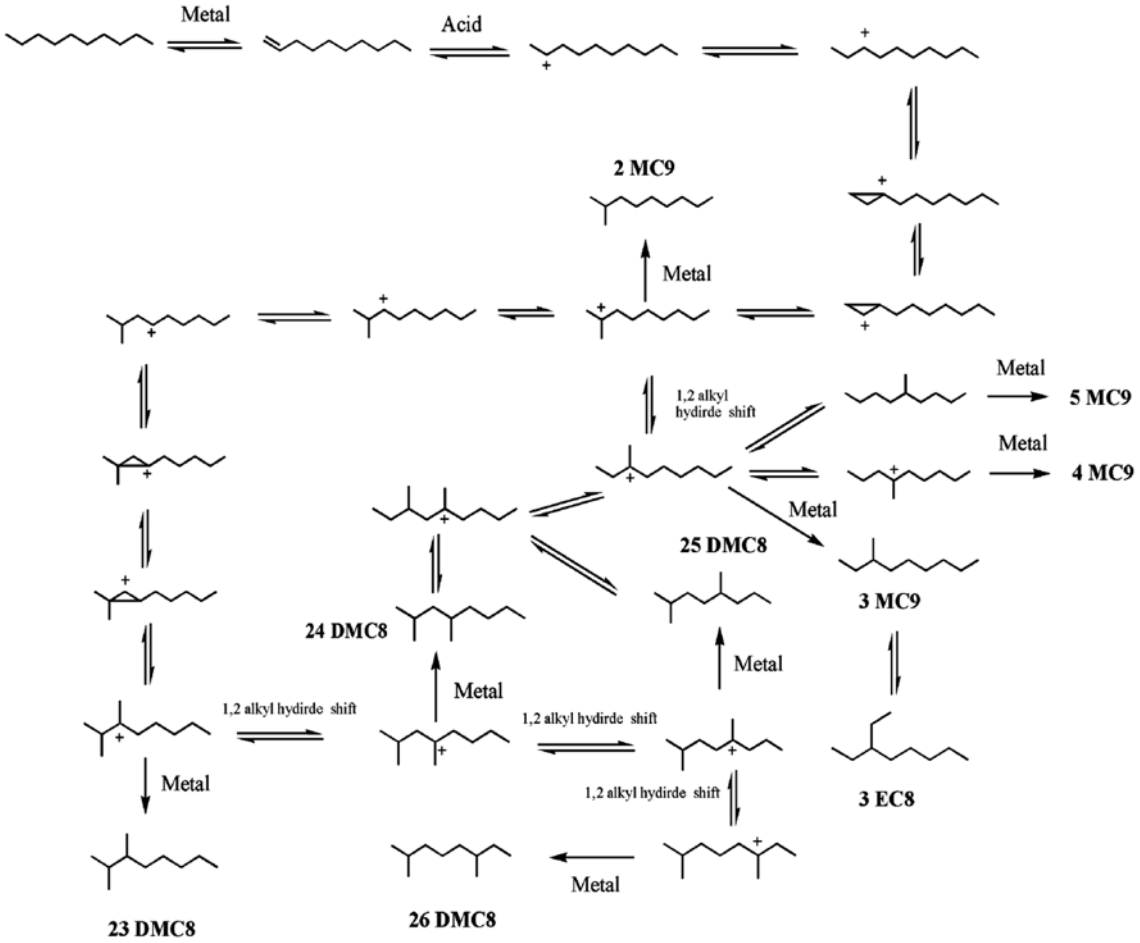

Scheme 1.

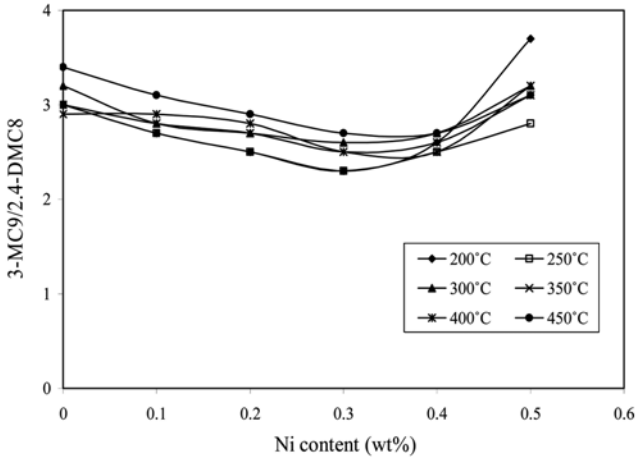

Fig. 9. Effect of Ni addition on the 3-MC9/2,4-DMC8 ratio over A series catalysts at different temperatures.

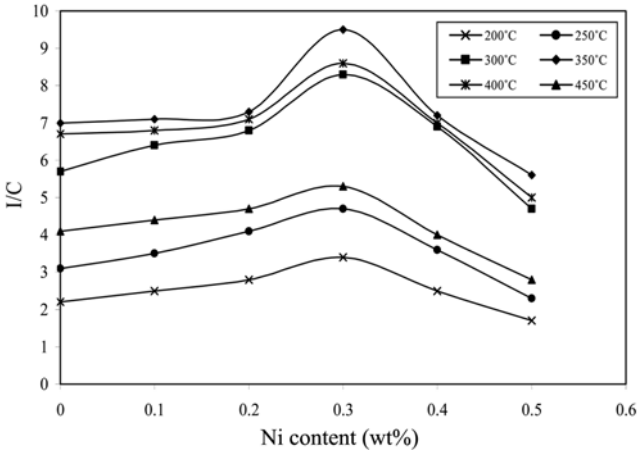

Fig. 10. Effect of Ni addition on the I/C ratio over A series catalysts at different temperatures.

nels of 12MR (5.7 Å×7.5 Å) and tortuous channel (6.5 Å×5.6 Å) with channel intersections [48]. The kinetic diameters of *n*-decane, monobranched and dibranched isomers are found in the following order: *n*-decane<monobranched<dibranched. Hence the formation of the dibranched isomers might be sterically hindered due to metallic particles present inside the pores.

2-4. Effect of Temperature on the 3-MC9/2,4-DMC8 Ratio

The effect of temperature on the ratios of the decane isomers over all the catalysts is illustrated in Fig. 9. The ratio of 3-MC9/2,4-DMC8 decreased (up to 400 °C) with the increase in the reaction temperature. It is generally considered that the branching of olefins occurs through the protonated cyclopropane intermediate as per the comprehensive description of carbenium ion rearrangement and cleavage by Weitkamp [44]. From the point of view of PCP mechanism, the isomerization of monobranched to dibranched decanes goes through secondary and tertiary carbocations, and therefore it should be thermodynamically favorable. The 3-MC9/2,4-DMC8 decreased with the increase in the temperature and Ni content up to the threshold value. The increase in the dibranched formation with increasing Ni content as well as temperatures indicates that the addition of Ni and higher reaction temperature favors the protonated cyclopropane intermediate mechanism, which is considered as slower than 1,2 alkyl hydride shift mechanism that leads to the formation of monobranched isomer again (Scheme 1). The enhancement in PCP mechanism can be accounted for in terms of better balance between metal particles formed and acid sites. Catalysts with high average metal particle sizes are found to be not favoring PCP mechanism, as the large particle size affects the development of better metal-acid balance. The unreduced Ni (shown by XPS), although not active in the dehydrogenation-hydrogenation step, might play a role on the isomerization of *n*-decane and also the ratio of the isomers formed. The decrease of 3-MC9/2,4-DMC8 ratio with increasing Ni content indicates that the Ni addition facilitates the dibranched formation through PCP intermediate and suppresses the faster 1,2 alkyl hydride shift, which usually leads to the formation of 3-MC9 from 2-MC9. Hence, the *n*-decane isomerization is considered to follow the mechanism of carbenium ion rearrangement and cleavage. According to comprehensive description of rules for carbenium ion rearrangement

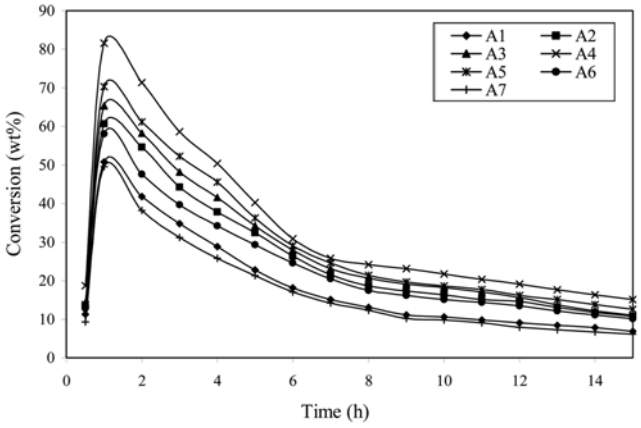

Fig. 11. Time-on-stream behavior of *n*-decane hydroisomerization over A series catalysts.

and cleavage given by Brouwer [49], the carbenium ion isomerizations that lead to a change in degree of branching occur through protonated cyclopropane (PCP) ring intermediate formation.

2-5. Effect of Ni Addition on I/C Ratio

The isomerization/cracking (I/C) ratio of an isomerization catalyst is an indication of its suitability for isomerization reactions. A good isomerization catalyst must have very high I/C ratio. In Fig. 10, an increasing trend in I/C ratio is observed up to the Ni addition of A_4 catalyst. Further Ni addition decreases the I/C ratio, indicating the higher cracking activity of larger bimetallic particles. Overall, the catalytic systems have decreased I/C ratio with increasing temperature, indicating that higher temperatures favor cracking.

2-6. Effect of Time on Stream

A time-on-stream study for a period of 15 h at 400 °C was carried out over all the catalysts in order to examine their sustainability. The results are shown in Fig. 11. All the catalysts showed large decreases in conversion with increasing reaction time up to 7 h, thereafter small decreases up to 15 h. Minimum fall in conversion occurred over A_4. Catalysts without Ni (A_1) and Ni only loaded (A_7) showed maximum fall in activity during the time on stream. The higher sustainability of A_4 is explained in terms of catalytically active

bimetallic particle formation and better balance between metal-acid sites. The fall in activity of the catalysts can be accounted for in terms of coke formation by which the active sites of the catalysts might be blocked.

Another reaction like time-on-stream was carried out for the formation of coke on catalyst surface. 8.89 g of reactant was fed onto 1 g of the A_4 catalyst and this was left on-stream for 15 h. It showed that 5.50 g (61.87%) of reactant was converted to products at the end of 15 h on stream. In the remaining 3.39 g (38.13%) of reactant, 2.19 g (24.63%) was transformed into coke, and 1.20 g (13.5%) of reactant might be converted to C_1-C_4 gaseous products.

CONCLUSIONS

The XRD patterns of commercial β-zeolite confirm their good crystallinity and structure. The XRD analysis shows that the crystallinity of the zeolite decreases with increasing Ni loading. The TEM analysis shows the formation of bimetallic (Ni-Pd) particles of nanoscale size. The XPS study reveals that complete reduction of Ni up to 0.3 wt% over 0.1 wt% Pd loaded β-zeolite. The TPR results show a decrease in Pd reduction temperature with increase Ni concentration. The acidity measurements by TPD-NH_3 studies show that some of the acid sites are occupied by the added Ni species. Because of the best metal-acid balance between bimetallic particles and acid sites of the support, catalyst A_4 shows an enhanced activity, dibranched isomers selectivity and sustainability of the catalysts in *n*-decane hydroisomerization. Further Ni addition leads to a fall in activity of the catalysts. Also, the β-zeolite based catalysts are found be more suitable catalysts for *n*-decane hydroisomerization.

ACKNOWLEDGEMENT

The authors gratefully acknowledge the catalyst characterizations and product analysis support from Chennai Petroleum Corporation Limited (CPCL), Chennai, India.

REFERENCES

1. S. J. Miller, *Stud. Surf. Sci. Catal*., **84**, 2319 (1994).
2. J. Weitkamp, *Appl. Catal*., **8**, 123 (1983).
3. P. A. Jacobs, M. A. Martens, J. Weitkamp and H. K. Beyer, *Faraday Discuss. Chem. Soc*., **72**, 353 (1981).
4. L.-J. Leu, L.-Y. Hov, B.-C. Kang, C. Li, S.-T. Wu and T.-C. Wu, *Appl. Catal*., **69**, 49 (1991).
5. M. Guisnet, V. Fouche, M. Belloum, J. P. Bournonville and C. Travers, *Appl. Catal*., **71**, 283 (1991).
6. M. Hochtl, A. Jentys and H. Vinek, *J. Catal*., **190**, 419 (2000).
7. V. Ponec, *Catal. Rev. Sci. Eng*., **11**, 41 (1975).
8. W. M. H. Sachtler, *Catal. Rev*., **14**, 193 (1976).
9. J. C. Bertolini, B. Tardi, M. Abon, J. Billy, P. Delichre and J. Massardier, *Surf. Sci*., **135**, 117 (1983).
10. J. M. Dominguez, A. Vazquez, A. J. Renouprez and M. J. Yacaman, *Surf. Sci*., **75**, 101 (1982).
11. M. L. Coonradt and W. E. Garwood, *Ind. Eng. Chem. Prod. Res. Dev*., **3**, 38 (1964).
12. J. A. Martens, M. Tielen, P. A. Jacobs and J. Weitkamp, *Zeolites*, **4**, 98 (1984).
13. A. S. Arifulin, A. B. Vol-Epshtein, A. A. Krichko and M. K. Yulin, *Khimiya Tverdogo Topliva*, **5**, 122 (1976).
14. J. A. Martens, J. Perez-Pariente and P. A. Jacobs, *Acta Physica et Chemica*, **31**, 487 (1985).
15. J. A. Martens, J. Perez-Pariente and P. A. Jacobs, *Math. Phys. Sci*., **165**, 115 (1986).
16. A. Corma, A. Martinez, S. Pergher, S. Peratello, C. Perego and G. Bellusi, *Appl. Catal*., **152**, 107 (1997).
17. L. B. Galperin, *Appl. Catal*., **209**, 257 (2001).
18. L. B. Galperin, S. A. Bradley and T. M. Mezza, *Appl. Catal*., **219**, 79 (2001).
19. S. P. Elangovan, B. Christian and M. Hartmann, *Catal. Lett*., **80**, 35 (2002).
20. S. P. Elangovan and M. Hartmann, *J. Cata*., **217**, 388 (2003).
21. Y. Rezgui and M. Guemini, *Appl. Catal*., **282**, 45 (2005).
22. F. Dorado, R. Romero and P. Cãnizares, *Appl. Catal*., **236**, 235 (2002).
23. P. Cãnizares, A. De Lucas, J. L. Valverde and F. Dorado, *Ind. Eng. Chem. Res*., **36**, 4797 (1997).
24. M. M. J. Treacy and J. B. Higgins, *XRD powder patterns for zeolites*, Vth edition (2001).
25. G. Faherazzi, A. Benedetti, A. Martorans, S. Giuliano, D. Duca and G. Deganello, *Catal. Lett*., **6**, 263 (1990).
26. B. D. Cullity, *Elements of X-ray diffraction*, Addison Wasley Pub Co. New York, 284 (1978).
27. I. Eswaramoorthi and N. Lingappan, *Catal. Lett*., **87**, 133 (2003).
28. R. M. Jao, T. B. Lin and J. R. Chang, *J. Catal*., **161**, 222 (1996).
29. I. Eswaramoorthi and N. Lingappan, *Korean J. Chem. Eng*., **20**, 133 (2003).
30. A. de Lucas, P. Sánchez, A. Fúnez, M. J. Ramos and J. L. Valverde, *Ind. Eng. Chem. Res*., in press.
31. P. Cãnizares, A. de Lucas, F. Dorado, A. Durán and I. Asencio, *Appl. Catal*., **169**, 137 (1998).
32. C. M. N. Yoshioka, T. Garetto and D. Cardoso, *Catal. Today*, **107**, 693 (2005).
33. J. S. Feeley and W. M. H. Sachlter, *Zeolites*, **10**, 738 (1990).
34. M. Narayana, J. Michalik, S. Contarini and L. Kevan, *J. Phys. Chem*., **89**, 3895 (1985).
35. Ch. Minchev, V. Knazirev, L. Kosova, V. Pechev, W. Grunsser and F. Schimidt, in: L. V. C. Rees (Ed.), Proceedings of the Fifth International Conference on Zeolites, Heydon, London, 335 (1980).
36. S. Narayanan, *Zeolites*, **4**, 231 (1984).
37. S. Xiao and Z. Meng, *J. Chem. Soc. Faraday Trans*., **90**, 2591 (1994).
38. M. D. Romero, A. de Lucas, J. A. Calles and A. Rodriguez, *Appl. Catal*., **146**, 425 (1996).
39. W. Zhang and P. G. Smirniotis, *J. Catal*., **182**, 400 (1999).
40. M. H. Jordao, V. Simoes, A. Montes and E. Cardoso, *Stud. Surf. Sci. Catal*., **130**, 2387 (2000).
41. G. E. Giannetto, G. E. Perot and M. R. Guisnet, *Ind. Eng. Chem. Prod. Res. Dev*., **25**, 481 (1986).
42. P. N. Kuznetsov, *J. Catal*., **218**, 12 (2003).
43. M. Steijns, G. Froment, P. Jacobs, J. Uytterhoeven and J. Weitkamp, *Ind. Eng. Chem. Prod. Res. Dev*., **20**, 654 (1981).
44. J. Weitkamp, *Ind. Eng. Chem. Prod. Res. Dev*., **21**, 550 (1982).
45. J. A. Martens and P. A. Jacobs, *Theoretical aspects of heterogeneous catalysis* (J. B. Moffat, Ed.), Chap. 2, Catalysis Series, Van Nos-

trand Reinhold, New York (1990).
46. P. Meriaudeau, V. A. Tuan, F. Lelebvre, V. T. Nghiem and C. Naccache, *Micropor. Mesopor. Mater*., **22**, 435 (1998).
47. A. de Lucas, J. L. Valverde, P. Sanchez, F. Dorado and M. J. Ramos, *Appl. Catal*., **282**, 15 (2005).
48. Ch. Baerlocher, W. H. Meier and D. H. Olson, Vth edition, pub. Struc. Comm. IZA (2001).
49. D. M. Brouwer, in: R. Prins, G. C. A. Schult (Eds.), *Chemistry and chemical engineering of catalytic processes*, Sijthof and Noordhoff, Germantown, MD (1980).